ERDC TN-SWWRP-10-6
October 2010

Intelligent Adaptive Time-Step Control for Modeling Rapidly-Evolving Hydrodynamic Flows in Adaptive Hydraulics (ADH)

by Gaurav Savant, Charlie Berger, Tate O. McAlpin, and Jennifer N. Tate

PURPOSE: This System-Wide Water Resources Program (SWWRP) technical note presents the development and application of a pseudo-transient continuation inspired flow model of rapidly evolving hydrodynamic flows caused by dam and levee failures. This unstructured, implicit, finite element model relies on computed hydrodynamic residuals to automatically adjust the time step size. The result is an efficient and accurate prediction of both the speed and depth of shock waves as the dam-break flow passes over initially dry and wet land.

BACKGROUND: Accurate and efficient numerical modeling of flows initiated by rapidly varying hydrodynamic flows caused by dam and levee failures (DLFs) is a critical component of hydraulic and water resources engineering because of large increases in the flow volume routed through the water body, the wave fronts, and the rapid flooding of the banks. DLF problems will be used as examples of rapidly-varying hydrodynamic flows. Because these phenomena are concurrent, DLF problems are particularly challenging when compared to other hydrodynamic flows such as those forced through tides or river discharge/stage.

DLF-created flows have been modeled typically using explicit methods. Since the flows are changing rapidly, the time step is likely to be small. For many river flow conditions, implicit models are preferable because larger time steps can be used. The wavelengths/wave periods captured are long and larger time steps yield greater efficiency. Using unstructured meshes is also advantageous as they can be readily made to fit the domain and are quick to produce with modern grid generators. Turan and Wang (2007) and Sarma and Saikia (2006) have concluded that implicit finite element methods are computationally inefficient for DLF type flows. This inefficiency is primarily a result of solving the matrix problem generated by the unstructured mesh and the difficulty in choosing an accurate and stable time step. So their conclusions would apply to any unstructured implicit method. However, a method that judiciously chooses the proper time step size to prevent instability could logically yield an efficient unstructured-mesh implicit time method.

In this note the pseudo-transient continuation (PTC) developed for steady-state solutions (Kelley and Keyes 1998) is modified, so that it can be used in a dynamic setting to address DLF problems. In general, PTC is a predictor-corrector technique for temporal integration in which the time step is changed as the objective of the convergence nears a solution or variation tolerance (Coffey et al. 2004). The modification herein of PTC uses an unstructured implicit model developed for riverine applications to be efficiently applied to DLF problems.

Pseudo-Transient Continuation. PTC is a technique for computing steady state solutions for time dependent partial differential equations. This method employs adaptive time-stepping to integrate an initial value problem derived from a partial differential equation boundary value problem. The adaptive time-stepping continues until sufficient accuracy is reached to switch to a Newton iteration process. For steady-state applications of PTC, temporal accuracy is sacrificed in the final stages of the simulation in favor of rapid convergence towards the steady-state. In the initial stages though, the solution is temporally accurate. This idea of initial temporal accuracy in the PTC is used to efficiently simulate DLF problems.

Consider a problem of the type

$$\frac{\partial C}{\partial t} + \nabla \bullet \underset{\sim}{R}(C) = 0 \tag{1}$$

where C is the fluid flow property being solved for and R is the flux.

Assuming that an approximate solution, C_k has been calculated, one implicit Euler step with step size δ yields a nonlinear equation

$$C_{k+1} = C_k + \delta_k \left[\nabla \bullet R(C)_{k+1} \right] \tag{2}$$

Where, *k* represents the solution at the current time step and *k*+1 represents the solution at the next time increment.

One Newton iteration of Equation 1 results in

$$C_{k+1} = C_k - \left[\frac{I}{\delta_k} + \nabla \bullet R'(C)_k \right]^{-1} \left[\nabla \bullet R(C)_k \right] \tag{3}$$

The purpose of PTC in DLF-type applications is to provide the worst error after one Newton iteration.

DLF problems are not steady-state problems; therefore, the time step selection must be conservative to resolve the transient temporal terms. Switched evolution relaxation (SER) (Mulder and van Leer 1985) is a numerical technique for automatic time step selection and is dependent on a previous time step, a previous residual, and the residual after one Newton iteration at the present time, yielding the time step

$$\delta_k = \min \left[\delta_{k-1} \left\| (\nabla \bullet R_{k-1}) \right\| / \left\| (\nabla \bullet R_k) \right\|, \delta_{max} \right] \tag{4}$$

where $\| \ \|$ indicates the L_2 norm.

These combinations of a single Newton iteration and SER are referred to as the pseudo-transient continuation method for adaptive time-stepping as used by the authors. As a method of time

integration, PTC is a Rosenbrock method (Gear 1971). PTC can be thought of as a predictor-corrector method, with the temporal error acting as the predictor and a Newton corrector (Kelley and Keyes 1998). For a truly time-independent problem, the idea of PTC is to maintain the trajectory of the solution but not the accuracy. DLF problems are highly time-dependent, so the PTC method is modified to restrain the computed time step using the SER and to allow more than one Newton iteration. To restrain the time step size and to ensure temporal accuracy in DLF problems, SER was modified to use the time step size and residual at time t = 0. This modification is necessary because during DLF the propagation of the flood wave is equally if not more important than the state of the wave at a much further time ($t \to \infty$), and restraining the time step will ensure temporal accuracy of the solution. Therefore, the time step is restrained such that:

$$\delta_k = \min\left(\delta_0 \left\|(\nabla \bullet R_0)\right\| / \left\|(\nabla \bullet R_k)\right\|, \delta_{\max}\right) \tag{5}$$

Limiting the time step in this manner ensures that the selected time step is always restrained by the error encountered during a single Newton iteration at t = 0. Hence, the time step is not allowed to grow rapidly and cause solution drifting. The computed time step δ_k is then used as the time step size for regular Newton iterations to obtain the temporally-accurate next time level value of R. The computed δ_k is now used in the temporal integration. If the specified tolerance is not achieved, the 'δ_k' is quartered and the computation is repeated. The inclusion of the δ_k calculation step is computationally inexpensive and is worthwhile because it provides an estimate of what the time step size should be for the current computations instead of random, user-provided guesses or time steps calculated with another method. As a conclusion to this section we provide the following salient points:

1. PTC, as described in this technical note, consists of the Rosenbrock method and an adaptive time-stepping algorithm.

2. SER, as described in Equation 5, is used for adaptive time-stepping.

3. A Newton-Raphson iteration, as described in Equation 3, is used as a corrector.

Two-Dimensional Shallow-Water Model Description. The model used for this study is the two-dimensional (2D) shallow-water module of the US Army Corps of Engineers' unstructured finite element model ADaptive Hydraulics (ADH). Information about ADH can be accessed at *https://adh.usace.army.mil*.

The 2D shallow-water equations are obtained by vertically integrating the mass and momentum conservation equations while assuming incompressible flow and a hydrostatic pressure distribution. Neglecting shear stress and fluid pressure at the free surface, the 2D shallow water equations are written as

$$\frac{\partial Q}{\partial t} + \frac{\partial F_x}{\partial x} + \frac{\partial F_y}{\partial y} + H = 0 \tag{6}$$

where

$$Q = \begin{Bmatrix} h \\ uh \\ vh \end{Bmatrix} \tag{7}$$

$$F_x = \begin{Bmatrix} uh \\ u^2 h + \frac{1}{2} g h^2 - h \frac{\sigma_{xx}}{\rho} \\ uvh - h \frac{\sigma_{yx}}{\rho} \end{Bmatrix} \tag{8}$$

$$F_y = \begin{Bmatrix} vh \\ uvh - h \frac{\sigma_{yx}}{\rho} \\ v^2 h + \frac{1}{2} g h^2 - h \frac{\sigma_{yy}}{\rho} \end{Bmatrix} \tag{9}$$

and

$$H = \begin{Bmatrix} 0 \\ gh \frac{\partial z_b}{\partial x} + n^2 g \frac{u\sqrt{u^2 + v^2}}{h^{4/3}} \\ gh \frac{\partial z_b}{\partial y} + n^2 g \frac{v\sqrt{u^2 + v^2}}{h^{4/3}} \end{Bmatrix} \tag{10}$$

Here,

ρ = fluid density
u = flow velocity in the x-direction
v = flow velocity in the y-direction
h = flow depth
g = gravitational acceleration
z_b = riverbed elevation
n = Manning's roughness coefficient
σ = Reynolds stress

The Reynolds stresses 'σ,' where the first subscript indicates the direction, and the second indicates the face on which the stress acts, are due to turbulence. The Reynolds stresses are determined using the Boussinesq approach to the gradient in the mean currents:

$$\sigma_{xx} = 2\rho\nu_t \frac{\partial u}{\partial x} \tag{11}$$

$$\sigma_{yy} = 2\rho\nu_t \frac{\partial v}{\partial y} \tag{12}$$

and

$$\sigma_{xy} = \sigma_{yx} = 2\rho\nu_t \left(\frac{\partial u}{\partial y} + \frac{\partial v}{\partial x} \right) \tag{13}$$

where ν_t = kinematic eddy viscosity (which varies spatially).

The equations are discretized using the finite element method in which u, v, and h are represented as linear polynomials on each element.

The system of partial differential equations represented in Equation 6 is solved using the finite element method using the approach of Petrov-Galerkin that incorporates a combination of a Galerkin test function and a non-Galerkin component to control oscillations due to convection (Berger 1997). The weak form of the equations is

$$\sum_e \left[\int_{\Omega_e} \left(\psi_i \frac{\partial Q}{\partial t} - \frac{\partial \phi_i}{\partial x} F_x - \frac{\partial \phi_i}{\partial y} F_y + \varphi_i A \frac{\partial Q}{\partial x} B \frac{\partial Q}{\partial y} + \psi_i H \right) d\Omega_e + \int_{\Gamma_e} \phi_i \left(F_x n_x + F_y n_y \right) dl \right] = 0 \tag{14}$$

where the variables have discrete values and

e = subscript indicating a particular element
Ω = domain
$\psi_i = \varphi_i I + \varphi_i$ = test function
ϕ_i = Galerkin test function
I = identity matrix
φi = non-Galerkin part of test function
$(n_x, n_y) = \hat{n}$ = unit outward normal to the boundary Γ_e

and

$$A = \frac{\partial F_x}{\partial Q} \tag{15}$$

$$B = \frac{\partial F_y}{\partial Q} \tag{16}$$

The temporal derivatives are expressed as

$$\left(\frac{\partial Q}{\partial t}\right)_j^{k+1} = \alpha \left[\frac{\left(\frac{3}{2}Q^{k+1} - \frac{1}{2}Q^k\right) - \left(\frac{3}{2}Q^k - \frac{1}{2}Q^{k-1}\right)}{\delta_k} \right]_j + (1-\alpha)\frac{\left(Q^{k+1} - Q^k\right)_j}{\delta_k} \tag{17}$$

where

j = nodal location
α = temporal factor

An α equal to one yields a second order approximation while a value of zero yields a first order approximation.

The system of nonlinear equations is solved with the Newton-Raphson iterative method for non-DLF problems and with the PTC and Newton-Raphson for DLF problems. In the absence of PTC-SER, ADH determines the time step based on the success of the non-linear computations. The success of non-linear computations is determined by the tolerance limits specified. If the tolerance is achieved, the time step is modified according to the time step series specified by the user; if the tolerance is not achieved, the time step is quartered and the computations are attempted again.

Equation 6 is composed of two distinct terms: a temporal term and a spatial term. The change in the spatial term is an indication of the slope of the temporal term. Using this fact, the residual in the spatial terms is calculated for one Newton iteration to determine the L_2 norm used in Equation 4.

TESTING: Tests were conducted to determine the behavior of ADH in replicating analytic test cases as well as simulated dam failure cases. The analytic cases simulated consisted of flow over a bump and supercritical shock. Two different flume experiments, 1D and 2D, involving simulations of dam failure were evaluated. A theoretical dam break case involving a hypothetical cylindrical column of water was also conducted. An actual dam break (Malpasset Dam Break) has also been simulated to gage the performance of PTC-SER-ADH. The computational time required for solution using PTC-SER modified ADH and ADH without the use of PTC-SER was also compared for the dam-break tests.

The first dam failure case is a straight-sloping flume in which a dam is instantaneously removed, producing a surge wave over initially-dry land. The second dam failure case is a flat flume with a straight reach connected to a 45º bend reach.

The PTC-SER-ADH tests were run before ADH tests without PTC-SER. The time step information from the PTC-SER-ADH tests was used to inform the maximum time step to be taken by the

ADH tests without PTC-SER. The presented results are from simulations where PTC-SER-ADH and ADH predicted hydrodynamic were the same.

All tests were performed on a personal computer with a single Intel Pentium 4 processor (3.4 GHz), and 4 GB of RAM.

Analytical Test Case 1: Flow over a Bump. The goal of this test is to determine the capability of the algorithm to accurately represent the transition between subcritical and supercritical flow. The parameters used for this test are those specified in Caleffi et al. (2007).

The spatial domain consists of a rectangular basin 25-m long by 1-m wide with bottom elevation represented by:

$$z_b = \begin{cases} 0 & \text{x} < 8\text{m} \\ 0.2\text{-}0.05\left(\text{x-}10\right)^2 & 8 \le \text{x} \le 12\text{m} \\ 0 & \text{x} > 12\text{m} \end{cases} \tag{18}$$

The discharge into the flow domain at the upstream boundary is 0.18 m^3/s, and the downstream water surface elevation is set at 0.33 m. The analytical solution is found through an application of Bernoulli's theorem. All figures and tables are provided in Appendices 1 and 2, respectively. Figure 1 illustrates the performance of the algorithm in representing the critical transition. As previously mentioned, PTC-SER-ADH and ADH results are the same. PTC-SER-ADH accurately replicates the analytical solution to the critical transition during flow over the bump specified in this problem.

The time step sizes were selected from considerations of stability. The initial time step size is the smallest step size with which the model converged and the largest step size was the largest step the model could take for temporal accuracy and still maintain stability. An indication of the initial time step is through computation of wave celerity.

$$\delta_0 = \Delta x / \sqrt{gh} \tag{19}$$

where

Δx = mesh element length
g = gravitational acceleration
h = initial reservoir water depth

Equation 19 essentially satisfies the Courant-Friedrichs-Lewy condition, and assures that the time step will be the explicit time step at the beginning of the simulation.

Analytical Test Case 2: 2D Oblique Hydraulic Jump. The second test case considered is the interaction of supercritical flow with a convergent vertical wall (see Figure 2). This test case (reported in Choi et al. 2007) has a supercritical inflow boundary at a depth of 1.0 m with an inflow velocity 8.57 m/s solely in the x-direction. The flow at the outflow boundary is

supercritical, so no boundary conditions are specified at the downstream boundary. The analytical solution for this case is a downstream depth of 1.5 m with an x-velocity of 7.9556 m/s at the outflow boundary and a 30° angle between the shock and the wall. Figure 2 illustrates the domain and the performance of PTC-SER-ADH and ADH towards replicating this supercritical flow. As previously mentioned PTC-SER-ADH and ADH results are the same. PTC-SER-ADH results replicate the analytical solution exceptionally well.

Dam Failure Case 1: Straight Flume. The first dam failure tested is a comparison with a study conducted at the U.S. Army Engineer Research and Development Center (USACE 1960-1961). The flume is 121.9 m long and 1.2 m wide with a 0.0015 bed slope. The dam is 61 m from the inflow boundary. Initially, water is pooled upstream of the dam to a depth of 0.3048 m at the dam face, and the flume section downstream of the dam is dry. Data from the numerical and physical models were compared at the locations indicated in Figure 3.

The numerical mesh consisted of 1,200 elements and 755 nodes. The numerical domain is closed (no flow into or out of the model) and the upstream, downstream and side walls are impermeable. The Manning's *n* value for the simulation was set at 0.009. The initial time step and the maximum time step to be used in Equation 9 were 0.09 and 0.25 s, respectively.

Figures 4-9 show the results of the water-depth time histories for Stations 160, 191, 200, 225, 275 and 345. These station numbers are the distance along the flume in feet as indicated in Figure 3. The time of arrival of the surge wave in the numerical model, PTC-SER-ADH as well as ADH, agrees well with the flume observations. The biggest difference is seen at Station 200 where the model captures the drop off in the water level but under predicts the peak depth around 50 s into the simulation.

The downstream stations (225, 275 and 345) compare well but differ from the physical model results at some points. Overall, the numerical results are in close agreement with the observed data. At Station 275 the flood wave (surge) arrives approximately 5 s before the observed surge. The greatest error in the simulated depth (approximately 9%) occurs at Station 345, but the predicted surge arrives at the same time as the observed surge.

Table 1 provides a comparison of computational time required by ADH and PTC-SER-ADH to run till completion and provide the same hydrodynamic results.

Dam Failure Case 2: 45º Bend Flume. The second dam failure is a 2D flow case reported by Brufau and Garcia-Navarro (2000). The flume combines a square reservoir and an initially-wet channel containing a 45º bend and is shown in Figure 10. This test case is a particularly good because both the shock speed of the initial wave and the upstream moving hydraulic jump can be compared.

The dimensions of the flow domain are shown in Figure 10. The initial depth of the reservoir is 0.25 m, and the channel has an initial depth of 0.01 m. The Manning's *n* value reported in the study for the flume bottom and the side walls were 0.0095 and 0.0195, respectively. The initial and the maximum time step size for use with Equation 9 were 0.009 and 0.25 sec, respectively.

Observations were made at the nine points shown in Figure 11. Comparisons for locations P1, P2, P3, P4, and P5 are shown in Figures 12-16. Other locations show similar behavior. In general, the figures indicate good agreement between the PTC-SER-ADH predicted and observed depths and shock speeds. Experimental data show high-frequency oscillations which cannot be captured by means of the 2D shallow water equations with a hydrostatic-pressure assumption irrespective of the solution scheme utilized either explicit or implicit. These oscillations are due to vertical accelerations and the hydrostatic assumption inherent to all 2-D shallow water equations precludes the numerical schemes from adequately representing these. The observed wave reflected at the bend and the ADH-predicted wave celerity and depth are in excellent agreement at Stations P2 and P3. Table 2 provides a comparison of computational time required by ADH and PTC-SER-ADH to run till completion and provide the same hydrodynamic results.

Dam Failure Case 3: Cylindrical Dam Break. This test case considers the behavior of a slumping 10-m column of water with an initial radius of 11 m into a quiescent 1-m deep body of water (Alcrudo 1993). The domain for this test case is represented in Figure 17. This case is an axis-symmetric problem and consequently one would expect symmetry in the solution as the mass of water slumps into the surrounding body of water. This problem does not render an analytically exact solution, but does provide a robust test case to check the ability of the algorithms in maintaining solution symmetry. Figures 18-21 graphically illustrate the performance of PTC-SER-ADH in capturing the symmetry of the solution. Table 3 provides a comparison of computational time required by ADH and PTC-SER-ADH to run till completion and provide the same hydrodynamic results.

Dam Failure Case 4: Malpasset Dam Break. The Malpasset dam failed explosively on December 2, 1959. The resulting flood wave was approximately 40-m high and destroyed infrastructure including three transformers labeled A, B, C in Figure 22. The time of failure of these transformers are known and were used along with other observed data to validate the performance of the PTC-SER-ADH and ADH models.

The dam failure and the wave propagation have been widely studied to determine the maximum water surface elevations reached due to the flood wave. These maximum water surface elevations are labeled P1 to P17 in Figure 22. Experimental data are also available from a scaled physical model built at Laboratoire National d'Hydraulique in 1964. The scale of the undistorted model is 1:400. The observations from this model are numbered S6-S14 in Figure 22 with S1-S5 located in the reservoir.

The mesh constructed to simulate this dam failure consisted of approximately 30,000 nodes and 60,000 elements with a higher resolution provided in the narrow valley (Figures 22 and 23). The valley below the dam is considered completely dry and the water surface elevation behind the dam is assumed to be 100 m. These conditions have been used by several researchers and have provided accurate results of the flood wave and the water surface elevations (Valiani et al. 2002, and Schwanenberg et al. 2004). A constant Manning's n value of 0.025 is used for the entire domain. Sensitivity simulations with Manning's n values of 0.010 and 0.033 were also performed, but a value of 0.025 provided the most accurate results. The land cover in the domain mainly consists of grass and therefore a Manning's n value of 0.025 is within the accepted range for this terrain and land use.

Table 4 lists the simulated water surface elevations obtained from PTC-SER-ADH and ADH as well as the observed water surface elevations. Table 5 provides the travel time of the flood wave to the transformers. The predicted water levels in this test case are in excellent agreement with the observed data.

Comparison of PTC-SER-ADH with ADH. Comparison runs were conducted between ADH and ADH modified with PTC-SER to determine the efficiency of the PTC-SER-ADH model over the ADH model without utilizing PTC-SER. Computational times are shown for run parameters where the PTC-SER-ADH and ADH hydrodynamic results were the same. Tables 1, 2 and 3 tabulate the results of these runs for Dam Failure Case 1, Dam failure Case 2, and Dam Failure Case 3 respectively.

PTC-SER-ADH results show great improvements over the ADH without PTC-SER results. In Dam Break Case 1, to obtain the same hydrodynamic results PTC-SER-ADH required approximately 80% of the time required by ADH with similar time steps and the same number of maximum iterations. For Dam Break Case 2, the use of PTC-SER yielded even greater time efficiency and required about 40% of the time required by a similar ADH run without PTC-SER. Dam Break Case 3 also required only about 70% of the time required by a similar ADH run without PTC-SER. The Malpasset Dam Break test case provided a simulation-time reduction of approximately 43% when PTC-SER was used. The Malpasset Dam Break simulation utilizing PTC-SER-ADH required 10 minutes to run till completion on a single processor personal computer. Manual adjustment of the time step could improve the performance of ADH without PTC-SER; however, the benefit of using PTC-SER is that the optimum time step is chosen by the algorithm without user interaction.

CONCLUSIONS: The U.S. Army Corps of Engineers 2D hydrodynamic model, ADaptive Hydraulics (ADH) with Pseudo Transient Continuation (PTC) is being developed for application in the numerical simulation of dam failure/levee breach type of problems.

The numerical model was validated through comparisons with five separate studies involving analytical solutions and dam failure in a flume setting. PTC-SER-ADH performed exceptionally well in replicating the analytical test cases simulated and the model shows good agreement with the shock wave speeds and depths for surges over initially-dry land (Dam Break Case 1), and initially-wet land (Dam break Case 2). A real world dam break was also simulated with good agreement between the solution and measured data.

Run-time comparisons between PTC-SER-ADH and ADH show that the incorporation of PTC-SER into ADH provides increased time efficiency of as much as 60% over conventional ADH.

ACKNOWLEDGMENT. The experiments described and results presented in this paper were obtained through research sponsored by the U.S. Army Corps of Engineers System Wide Water Resources Program (SWWRP). Permission was granted by the Chief of Engineers to publish this information.

The authors are grateful to Dirk Schwanenberg for providing the Malpasset Dam Break bathymetric and observational data.

ADDITIONAL INFORMATION: For additional information, contact Dr. Gaurav Savant, Coastal and Hydraulics Laboratory, U.S. Army Engineer Research and Development Center, 3909 Halls Ferry Road, Vicksburg, MS 39180 at 601-634-3628, or e-mail: *Gaurav.Savant@usace.army.mil*, or Dr. Charlie Berger, Coastal and Hydraulics Laboratory, 3909 Halls Ferry Road, Vicksburg, MS 39180 at 601-634-2570, or e-mail: *Charlie.R.Berger@usace.army.mil*. This effort was funded through the System–Wide Water Resources Program (SWWRP). For information on SWWRP, please consult *https://swwrp.usace.army.mil/* or contact the Program Manager, Dr. Steven L. Ashby: *Steven.L.Ashby@usace.army.mil*.

This technical note should be cited as follows:

> Savant, G., R. C. Berger, T. O. McAlpin, and J. N. Tate. 2010. *Intelligent adaptive time-step control for modeling rapidly-evolving hydrodynamic flows in adaptive hydraulics (ADH)*. ERDC TN-SWWRP-10-6. Vicksburg, MS: U.S. Army Engineer Research and Development Center.

REFERENCES

Alcrudo, F., and P. Garcia-Navarro. 1993. A high-resolution Godunov-type scheme in finite volumes for the 2D shallow-water equations. *International Journal for Numerical Methods in Fluids*. 16: 489-505.

Berger, R. C. 1997. *HIVEL 2D v2.0 users manual*. Vicksburg, MS: U.S. Army Engineer Waterways Experiment Station.

Berger, R. C., and R. L. Stockstill. 1995. Finite element model for high velocity channels. *Journal of Hydraulic Engineering* 121(10), 710-716.

Brufau, P., and P. Garcia-Navarro. 2000. Two-dimensional dam break flow simulation. *International Journal for Numerical Methods in Fluids* 33, 35-57.

Caleffi, V., A. Valiani, and A. Zanni. 2003. Finite volume method for simulating extreme flood events in natural channels. *Journal of Hydraulic Research* 41(2), 2003:167-177.

Choi, B. Y., M. Iskandrani, J. Levin, and D. B. Haidvogel. 2004. A spectral finite-volume method for shallow water equations. *Monthly Weather Review* July: 1777-1791.

Coffey, T. S., C. T. Kelley, and D. E. Keyes. 2004. Pseudo-transient continuation and differential-algebraic equations. *SIAM Journal of Scientific Computing* 25:553-569.

Kelley, C. T., and D. E. Keyes. 1998. Convergence analysis of pseudo-transient continuation. *SIAM Journal of Numerical Analysis* 35, 508-523.

Gear, C. W. 1971. Numerical initial value problems in ordinary differential equations. Englewood Cliffs, NJ: *Prentice Hall*.

Mulder, W. A., and B. van Leer. 1985. Experiments with implicit upwind methods for the Euler equation. *Journal of Computational Physics* 59:232-246.

Sarma, A. P., and D. S. Saikia. 2006. Dam break hydraulics in natural rivers. *World Environmental and Water Resources Congress, ASCE Conference Proceedings* 200, 69(2006).

Schwanenberg, D., and M. Harms. 2004. Discontinuous Galerkin finite-element method for transcritical two-dimensional shallow water flows. *J. Hydraulic. Engineering* 130(5), 412-421.

Tate, J. N., R. C. Berger, and R. L. Stockstill. 2005. Refinement indicator for mesh adaption in shallow-water modeling. *Journal of Hydraulic Engineering* 132(8), 854-857.

Turan, B., and K.-H. Wang. 2007. Flood and shock waves simulation by using finite volume technique on unstructured meshes. *World Environmental and Water Resources Congress 2007*.

U.S. Army Engineer Waterways Experiment Station. 1960. Floods resulting from suddenly breached dams: Conditions of minimum resistance. Paper: 2-237, Report 1.

U.S. Army Engineer Waterways Experiment Station. 1961. Floods resulting from suddenly breached dams: Conditions of maximum resistance. Paper: 2-374, Report 2.

Valiani, A., V. Caleffi, and A. Zanni. 2002. Case study: Malpasset dam-break simulation using a two-dimensional finite volume method. *Journal of Hydraulic Engineering* 128(5):461-472.

APPENDIX 1

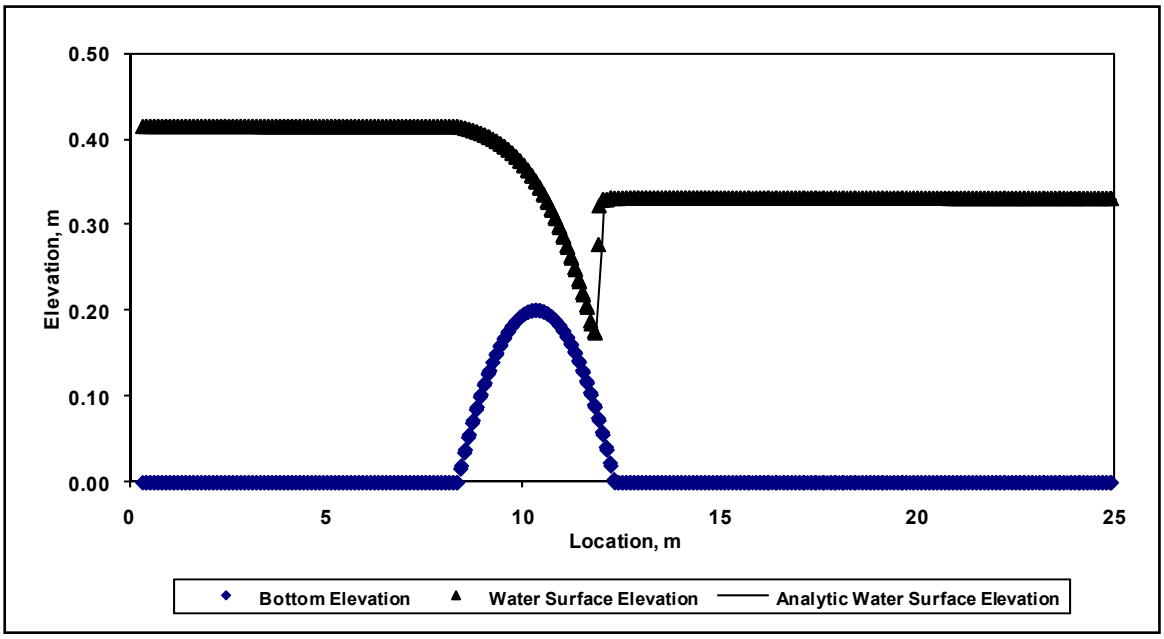

Figure 1. Analytical and computed water surface elevations.

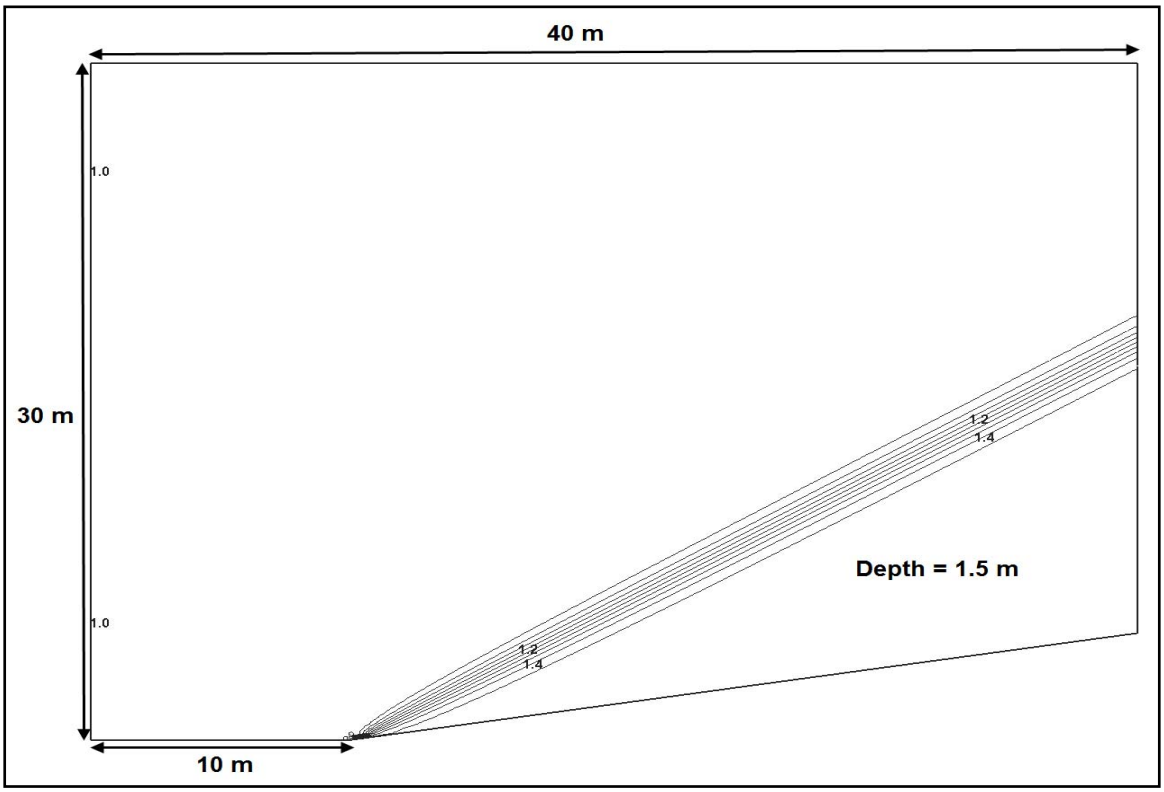

Figure 2. Domain and water depth contour results for analytical test case 2 (inflow is from the left hand side and outflow is at the right hand side).

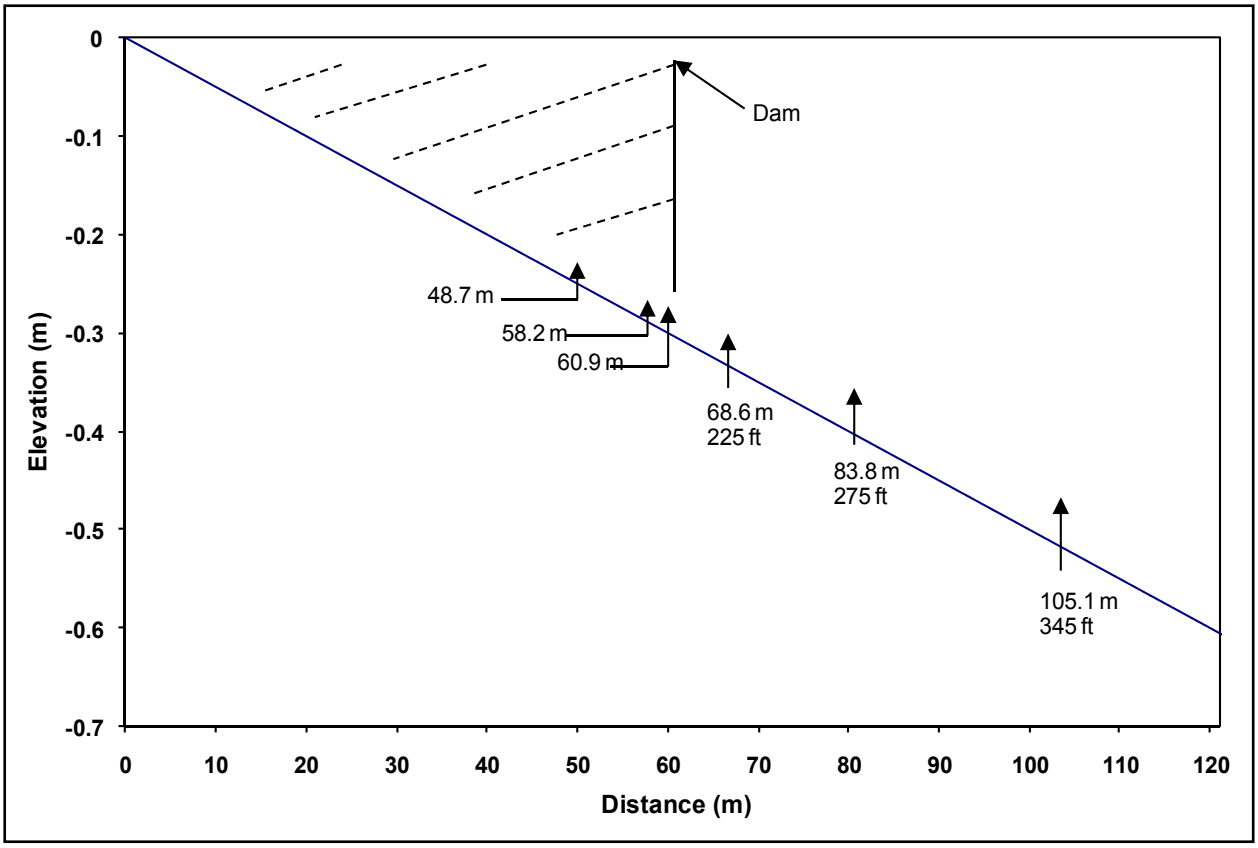

Figure 3. Layout of straight flume (elevation view) with observation stations (numbers under the metric locations indicate observation stations).

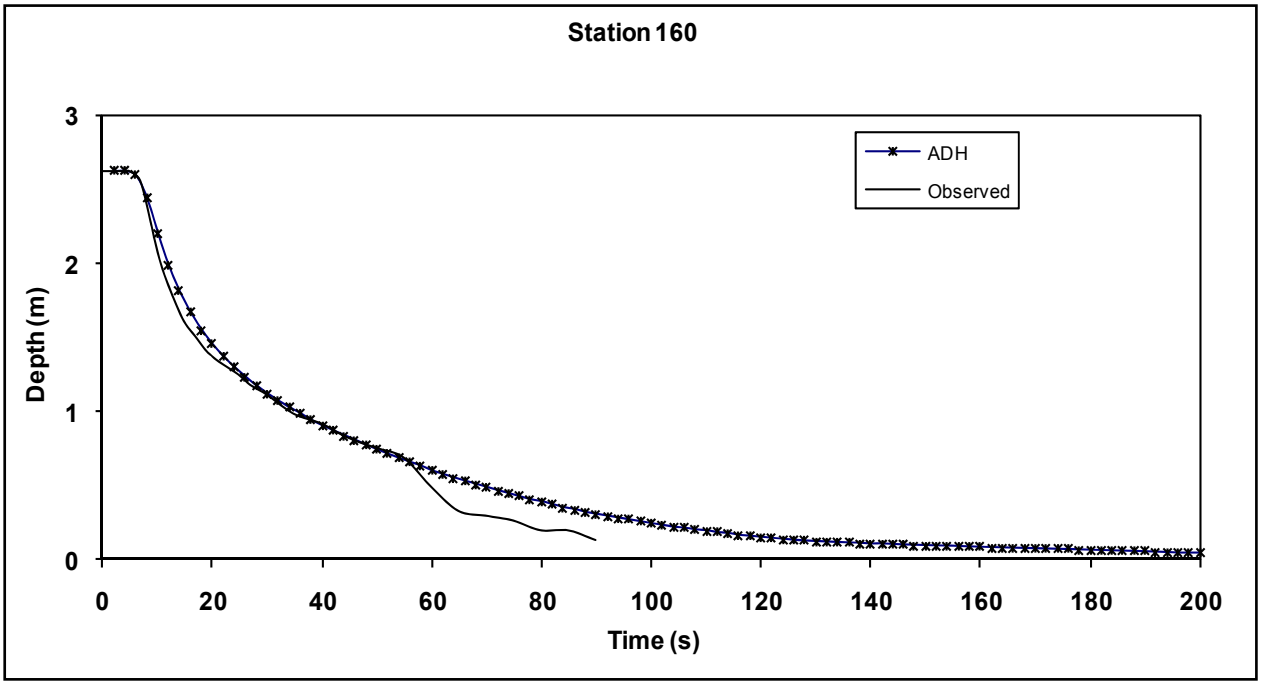

Figure 4. Depth comparison for ADH and flume experiment, sta 160.

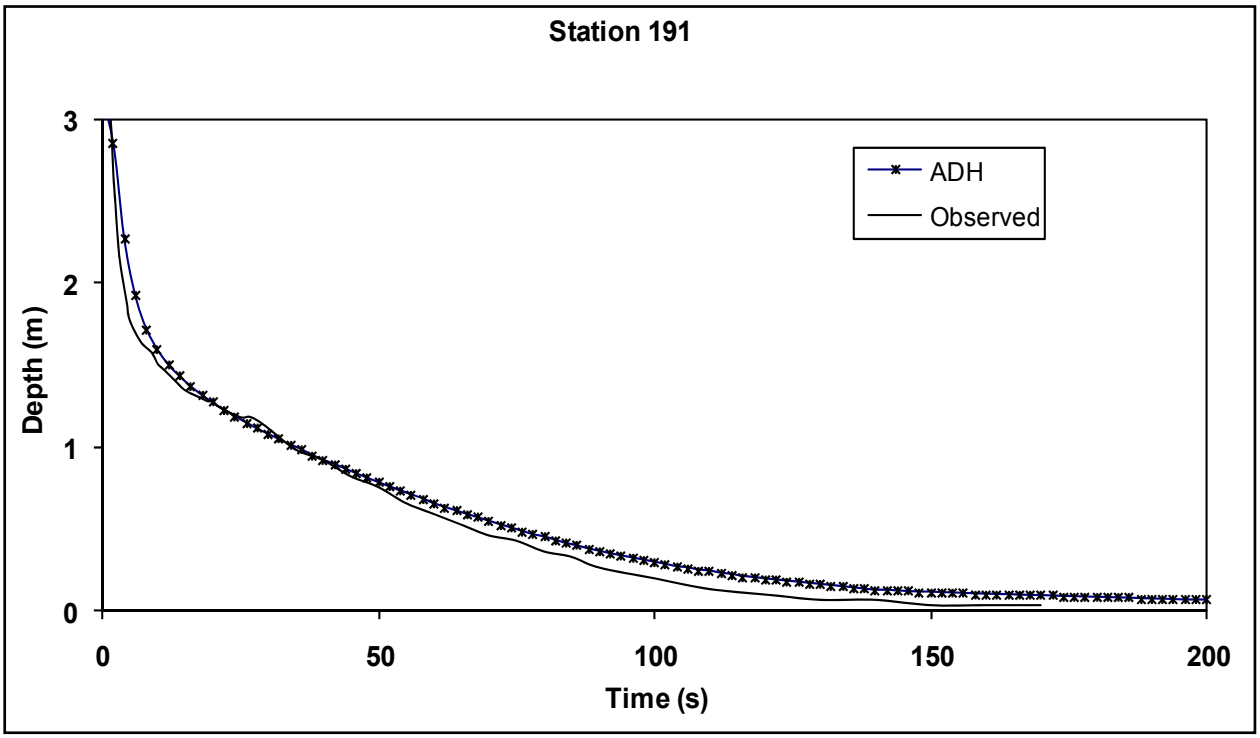

Figure 5. Depth comparison for ADH and flume experiment, sta 191.

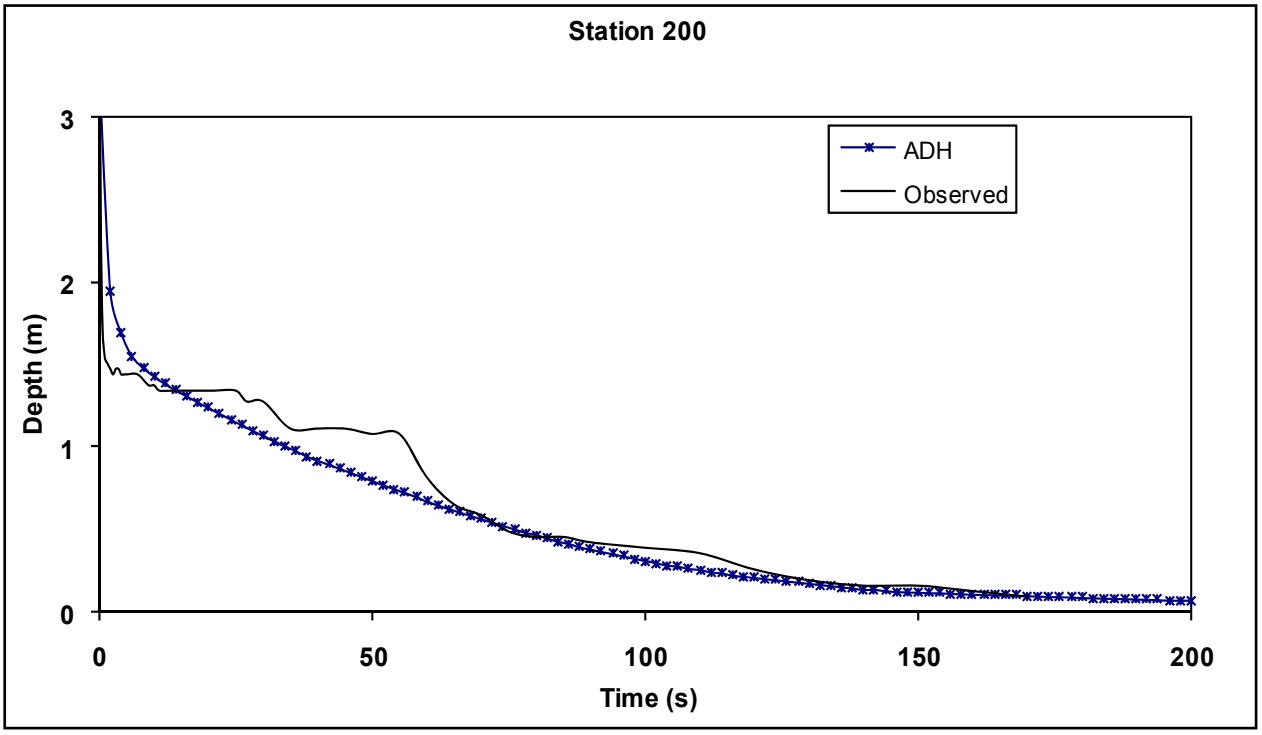

Figure 6. Depth comparison for ADH and flume experiment, sta 200.

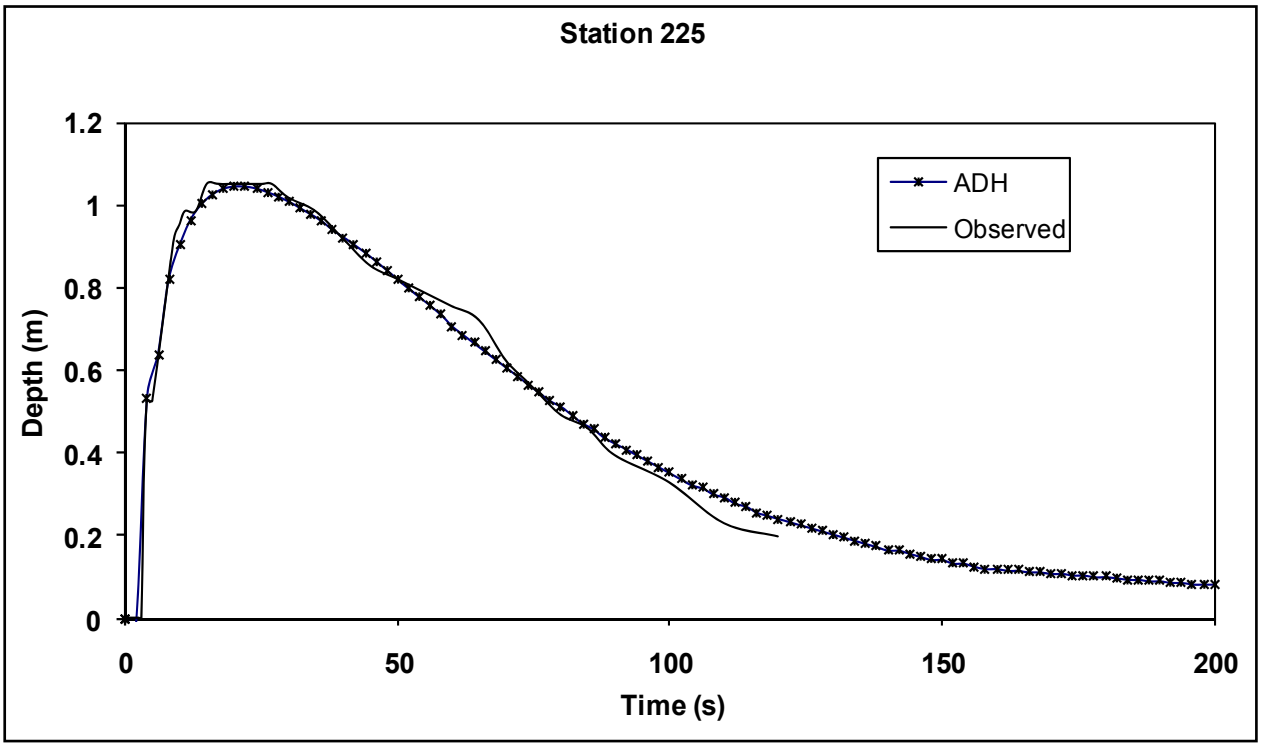

Figure 7. Depth comparison for ADH and flume experiment, sta 225.

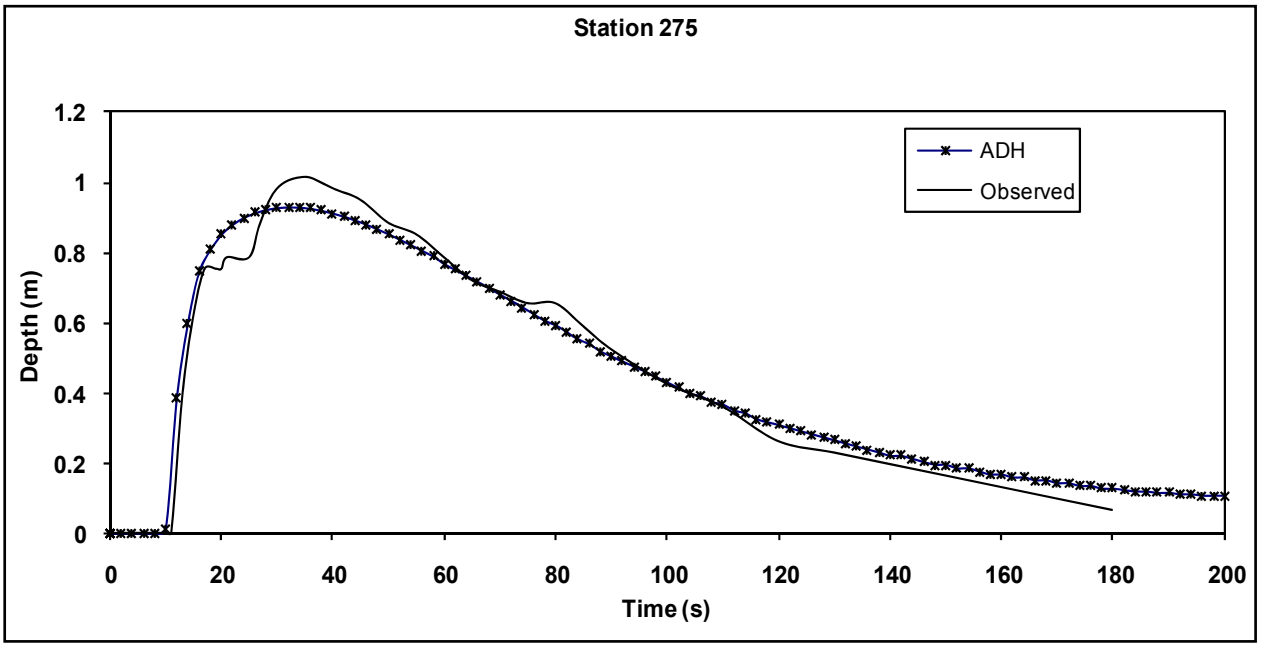

Figure 8. Depth comparison for ADH and flume experiment, sta 275.

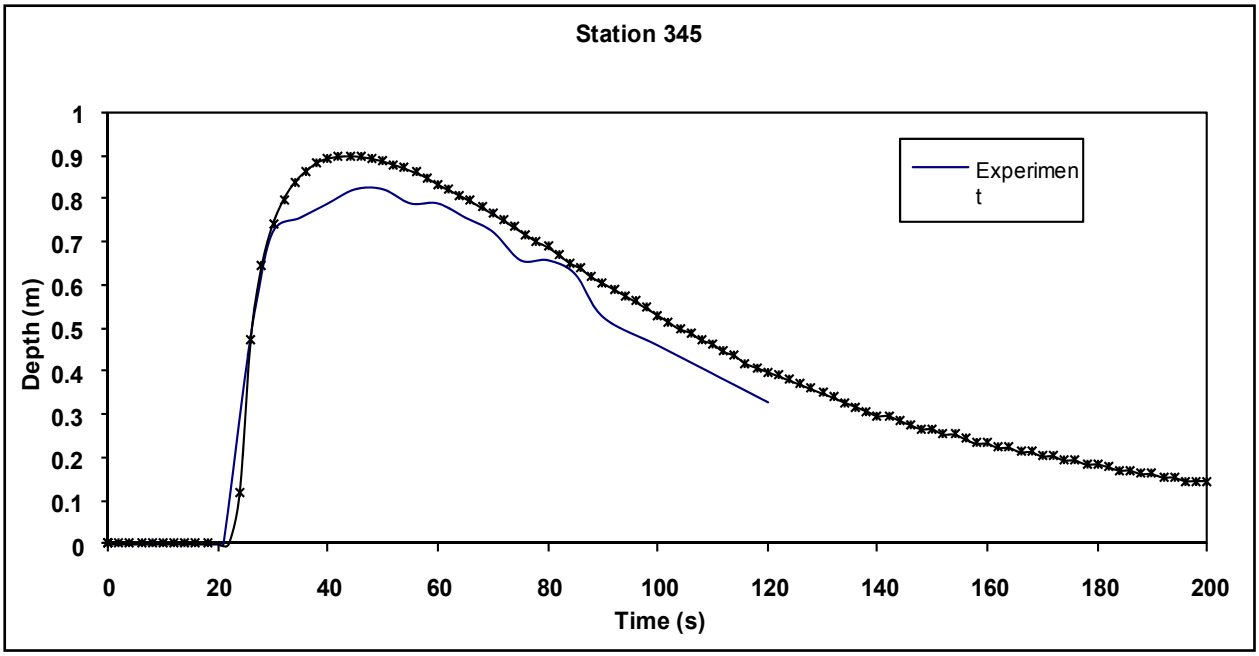

Figure 9. Depth comparison for ADH and flume experiment, sta 345.

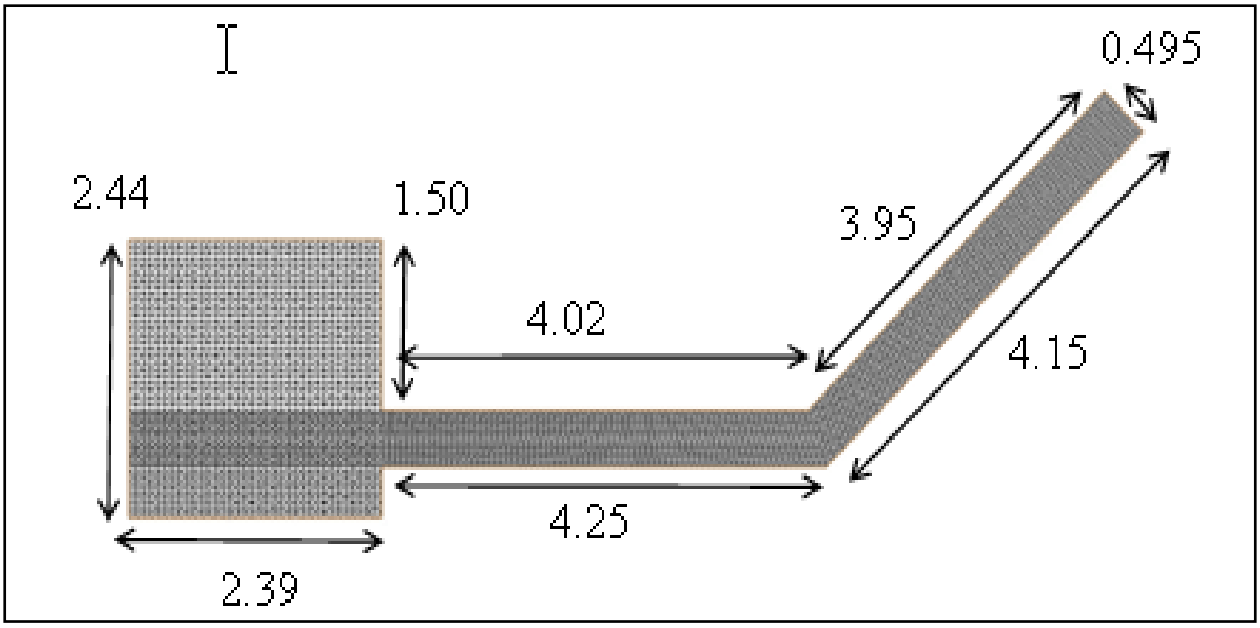

Figure 10. PLAN view of numerical test flume (all lengths are in meters).

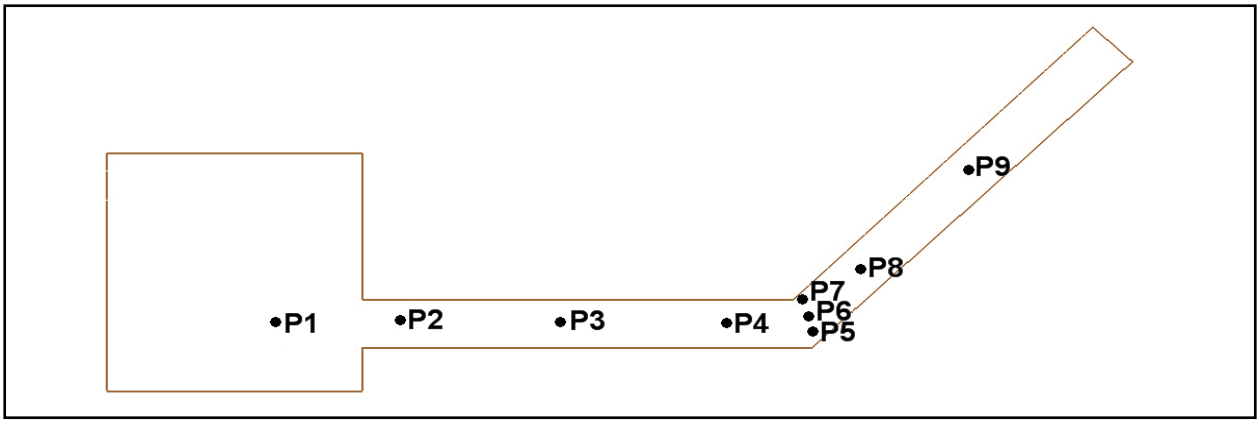

Figure 11. Observation points.

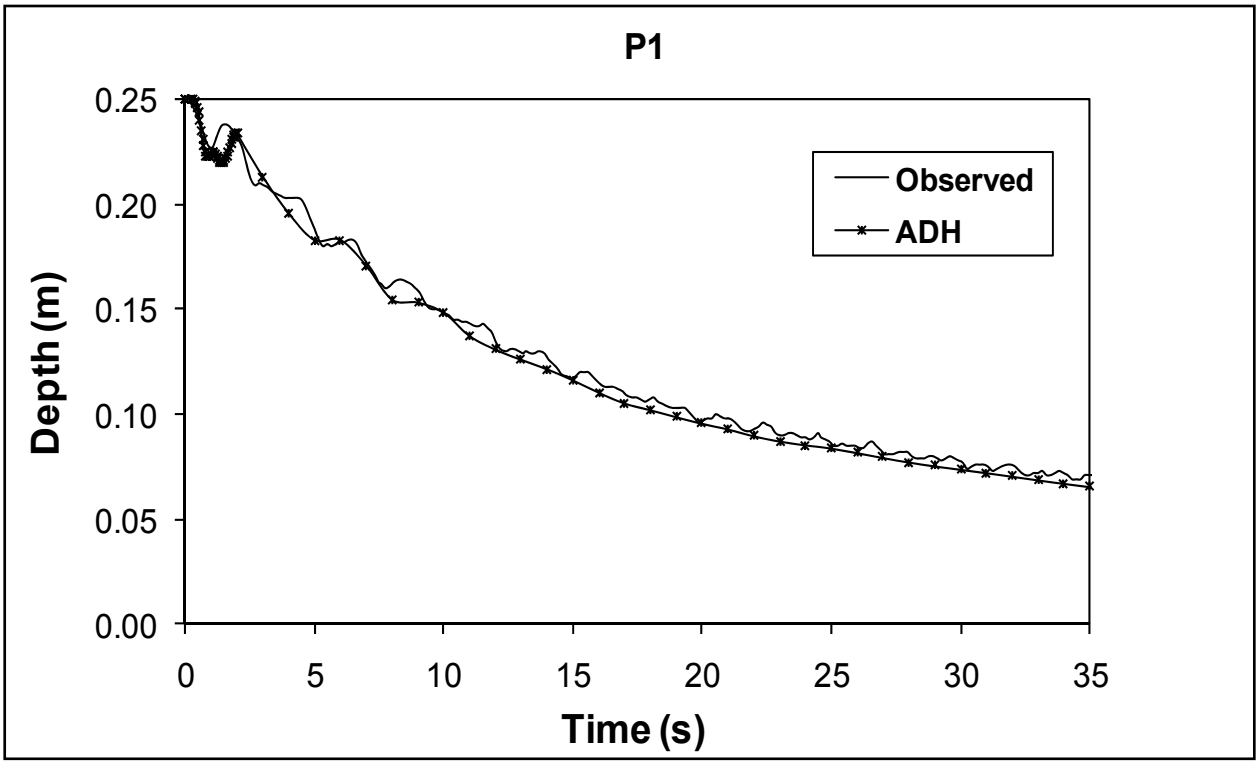

Figure 12. Depth comparison for ADH and flume experiment, sta P1.

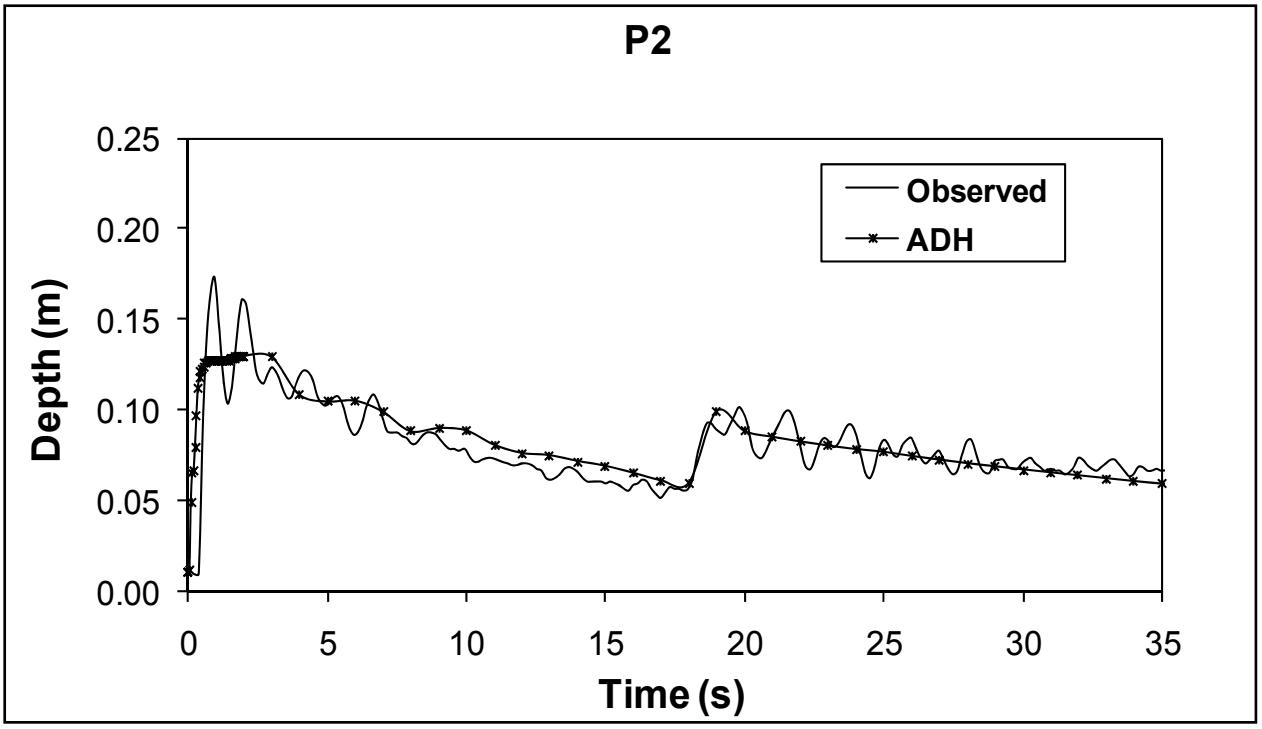

Figure 13. Depth comparison for ADH and flume experiment, sta P2.

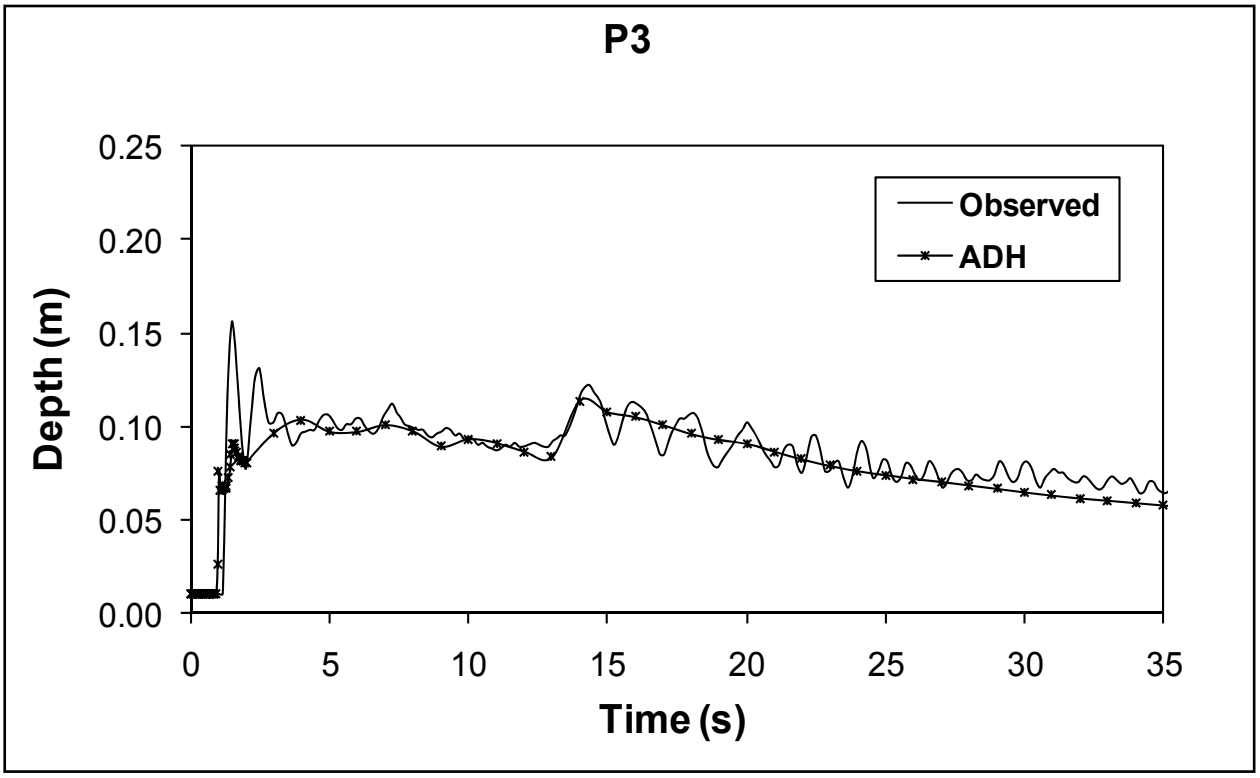

Figure 14. Depth comparison for ADH and flume experiment, sta P3.

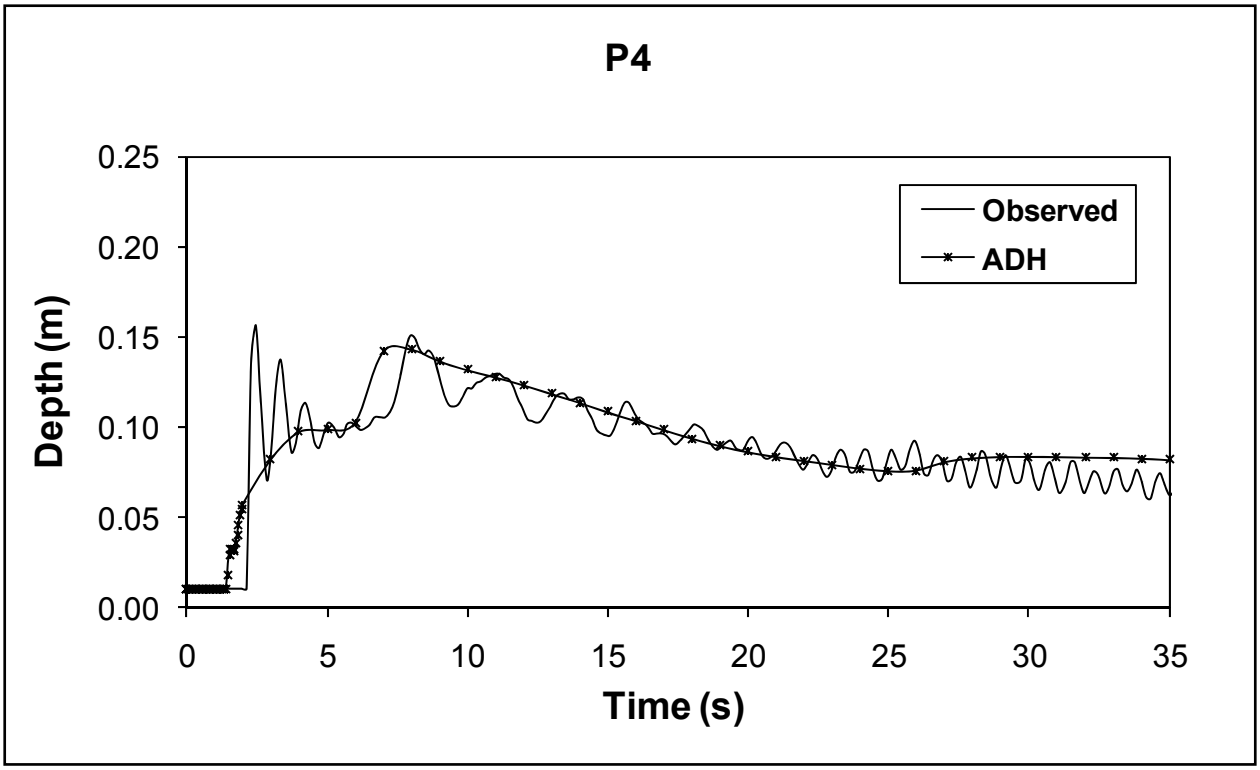

Figure 15. Depth comparison for ADH and flume experiment, sta P4.

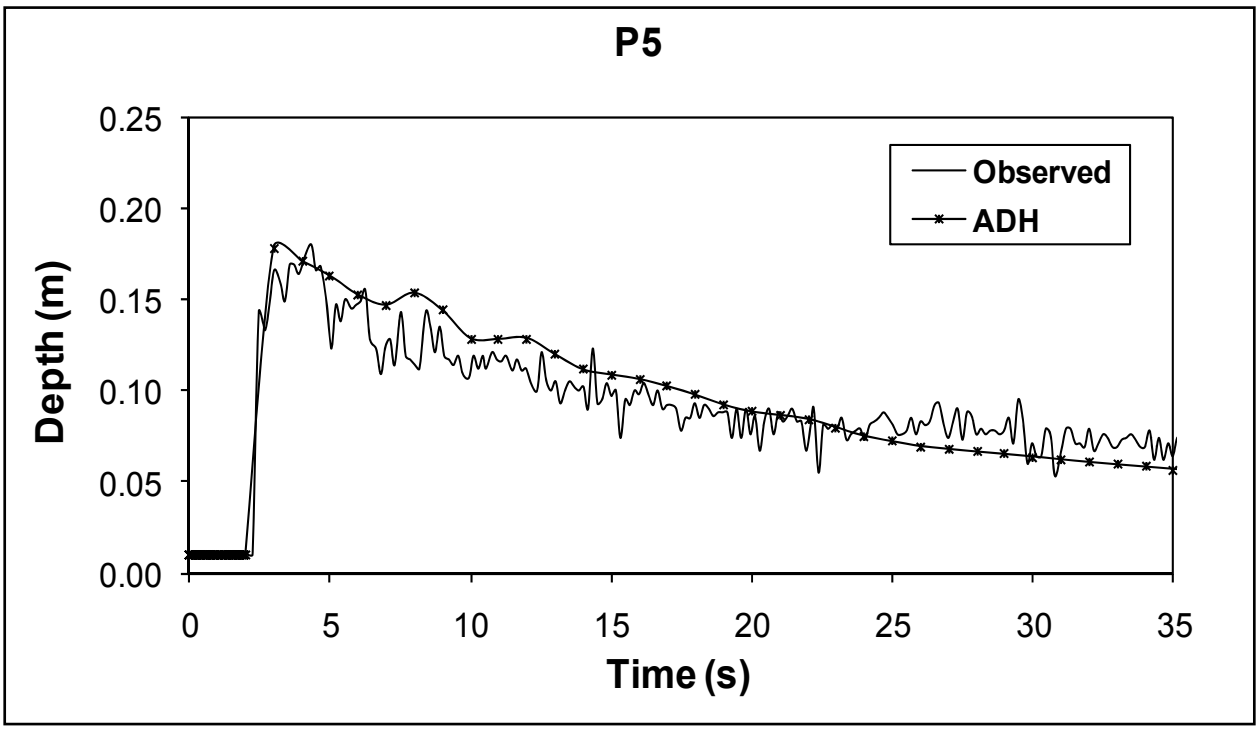

Figure 16. Depth comparison for ADH and flume experiment, sta P5.

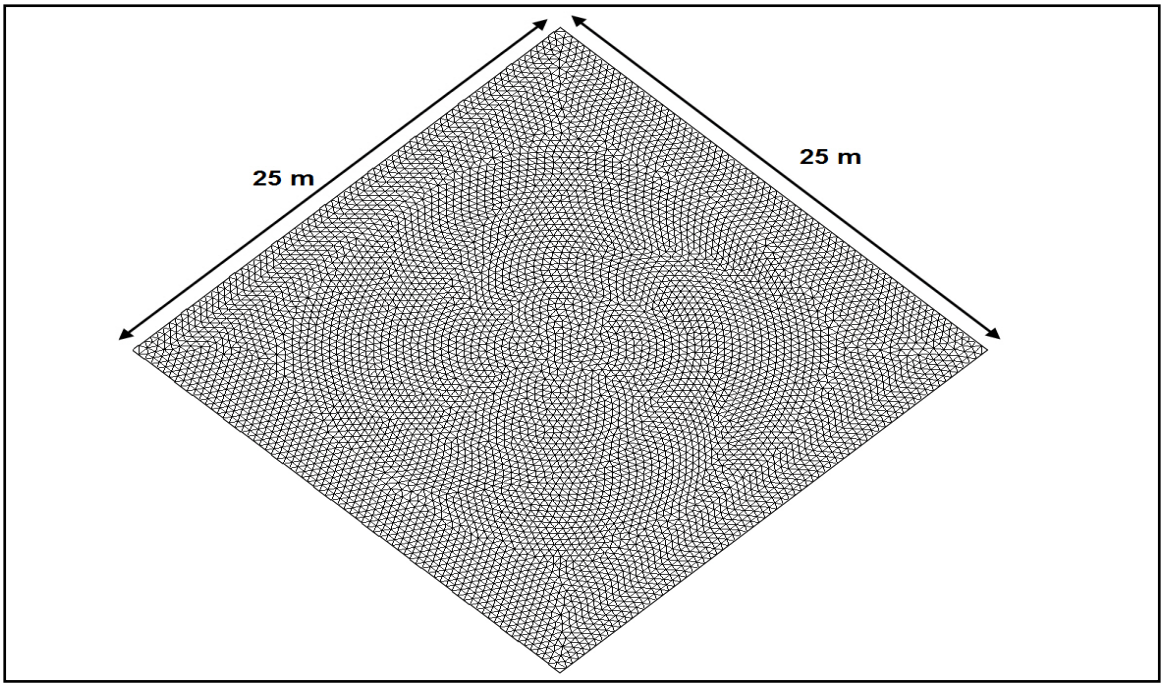

Figure 17. Domain for circular dam break test case.

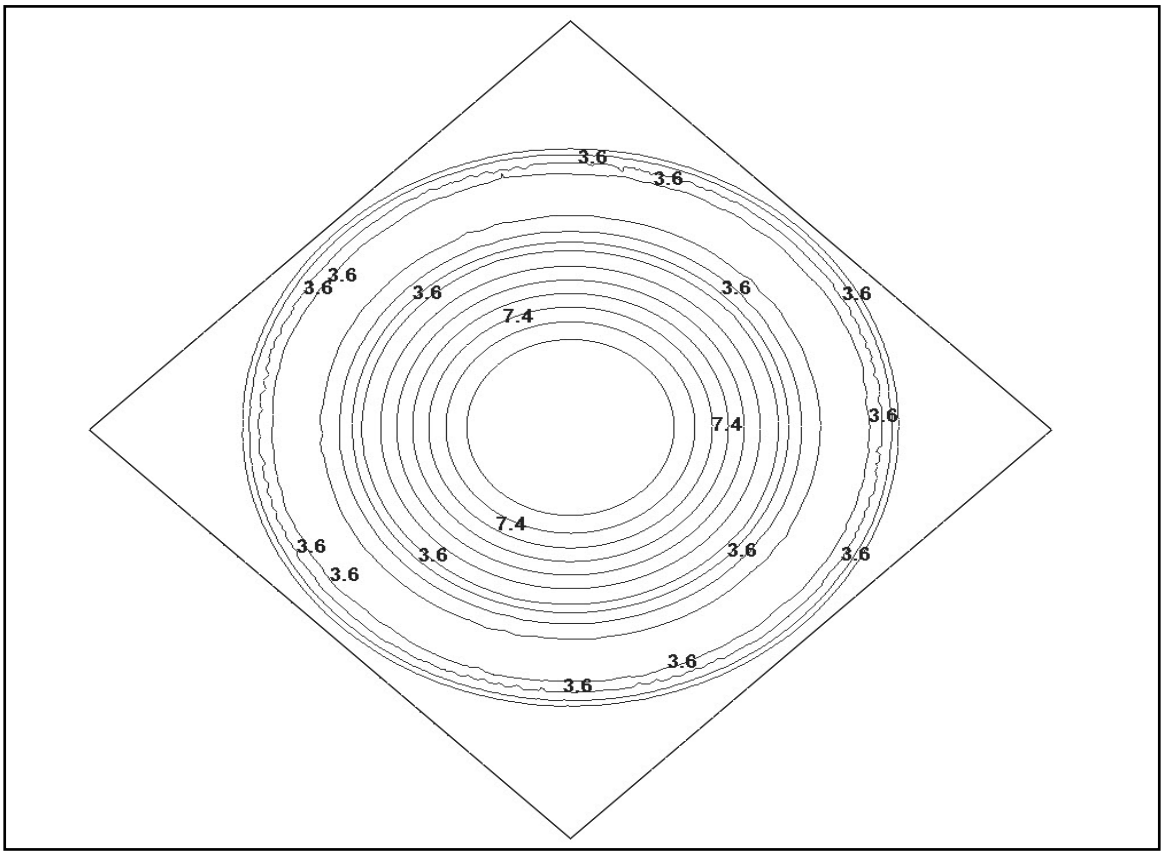

Figure 18. Water surface elevation (in meters) contours at 0.6 seconds circular dam break test case.

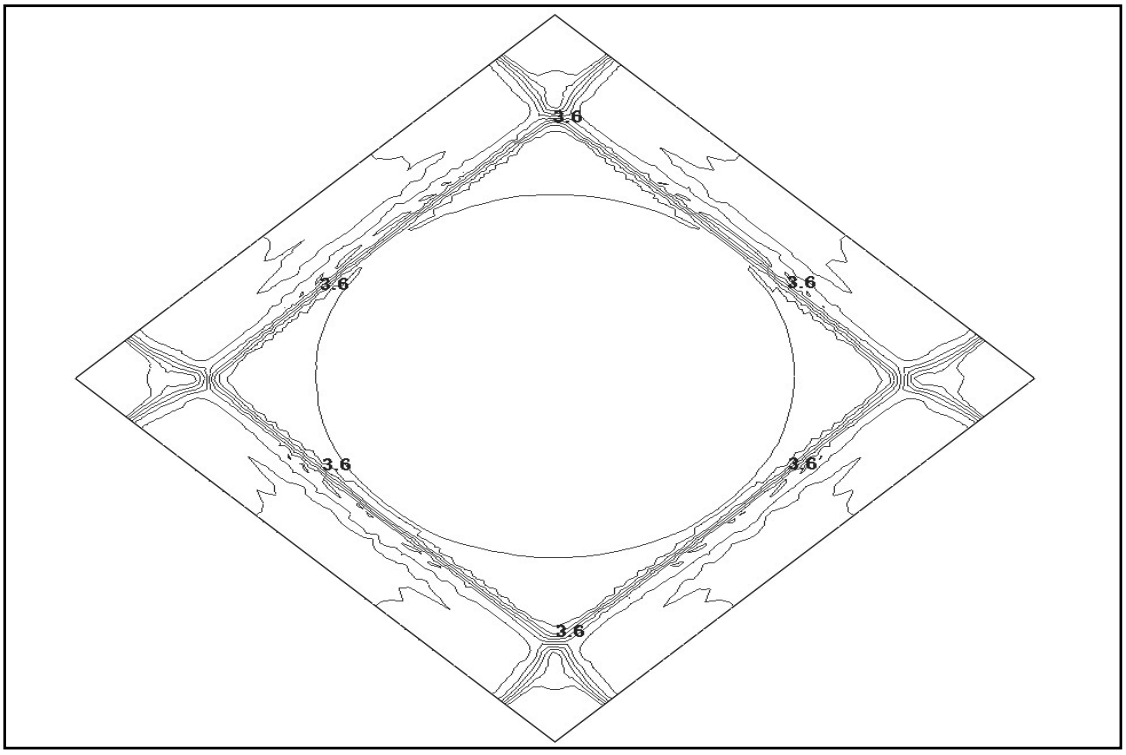

Figure 19. Water surface elevation contours at 2.0 seconds for circular dam break test case.

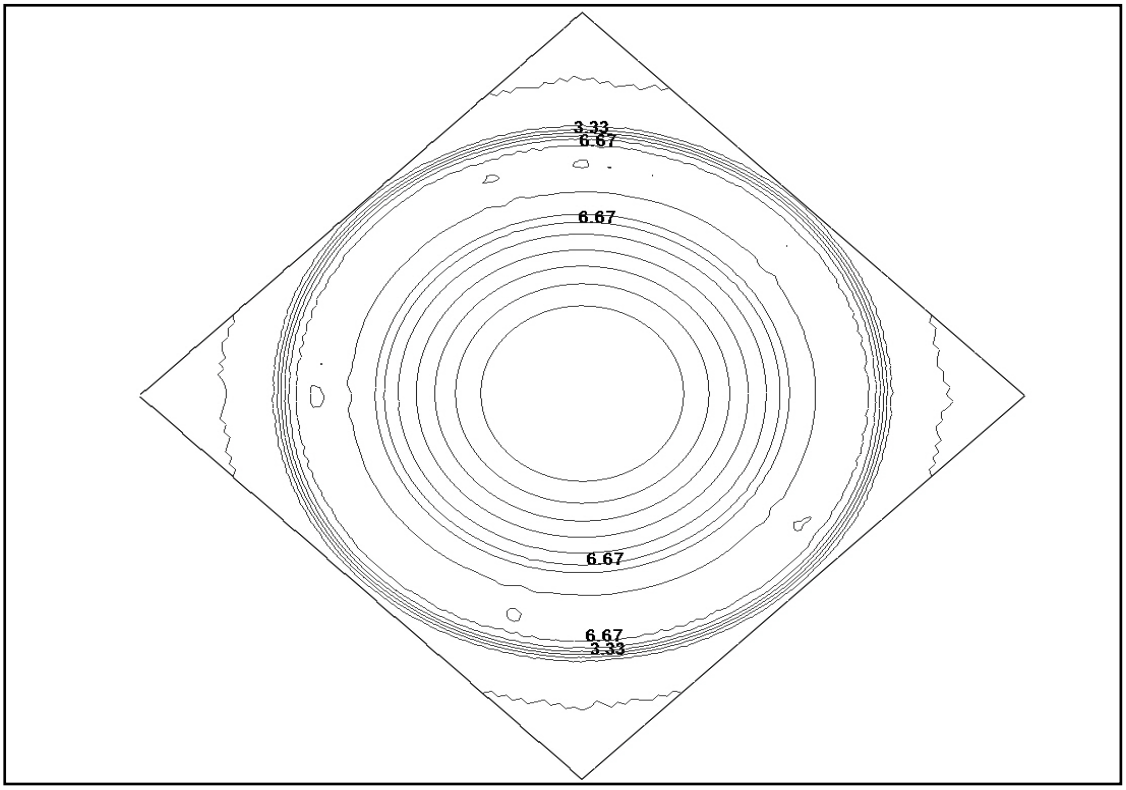

Figure 20. Velocity contours at 0.6 seconds for circular dam break test case.

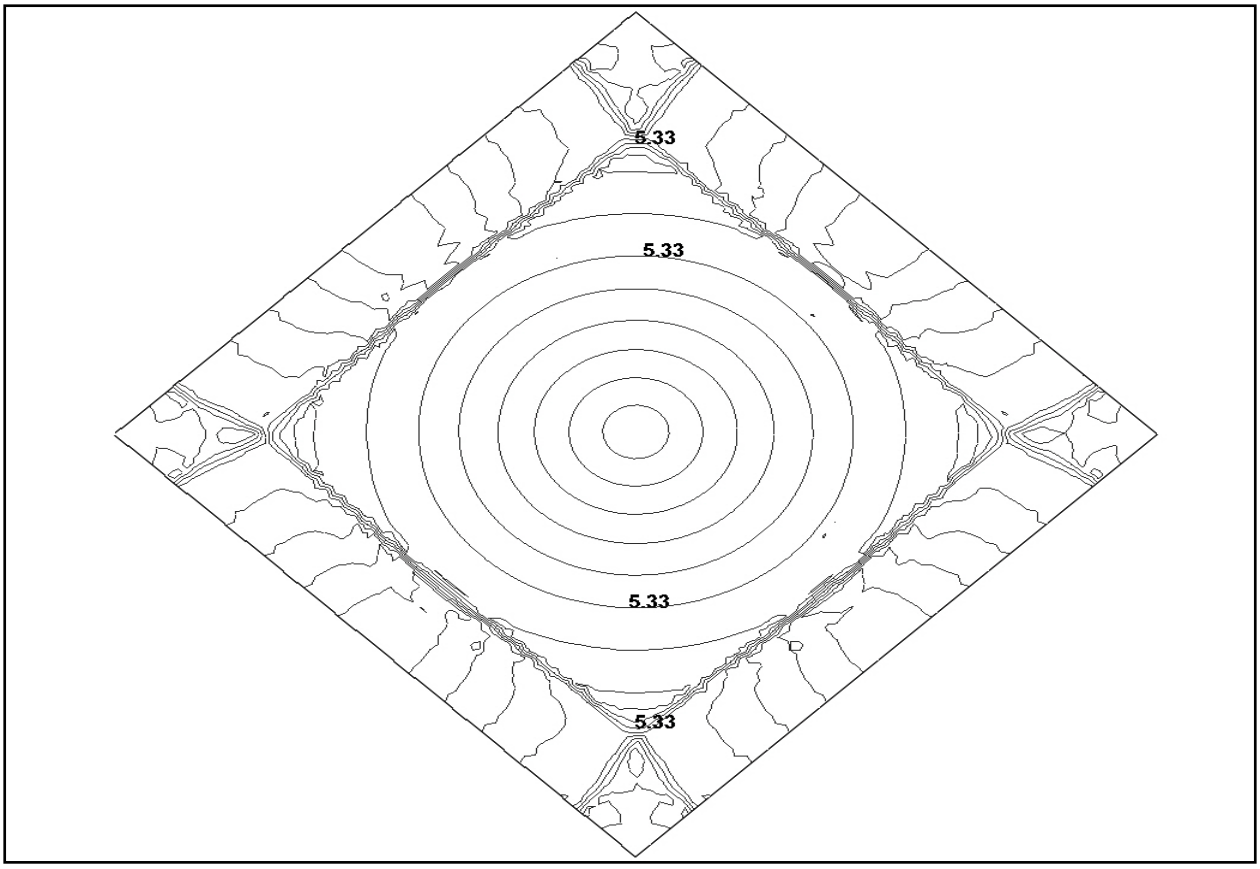

Figure 21. Velocity contours at 2.0 seconds for circular dam break test case.

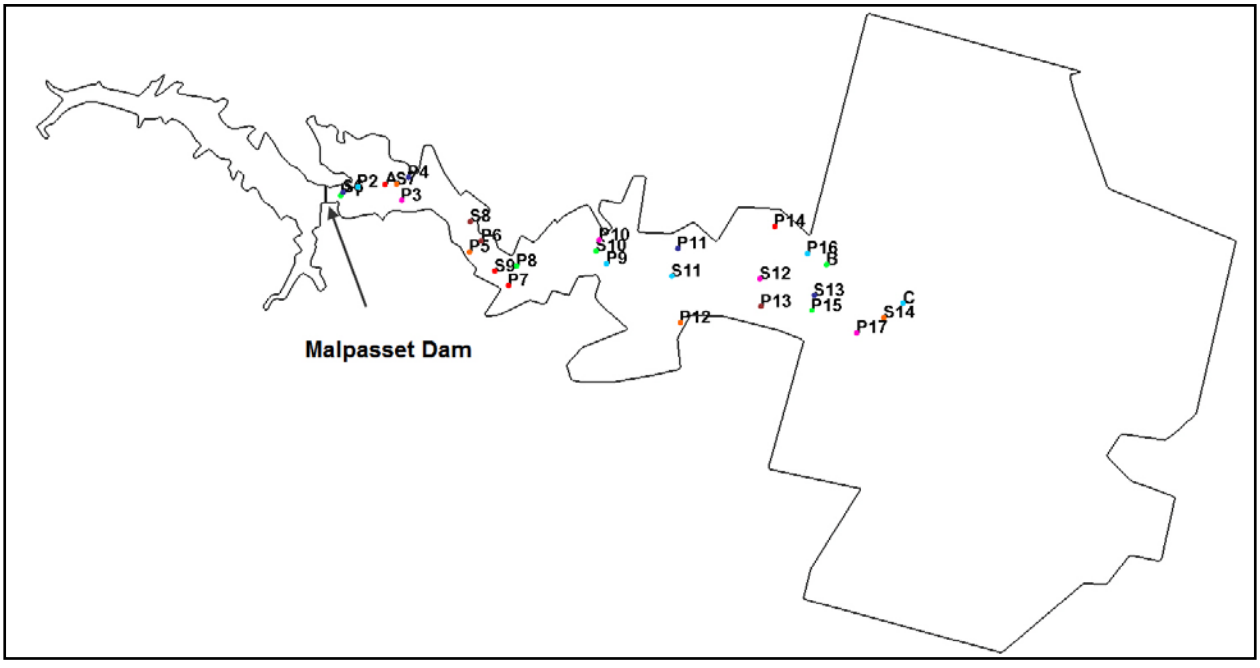

Figure 22. Malpasset dam domain showing location of dam and observation stations.

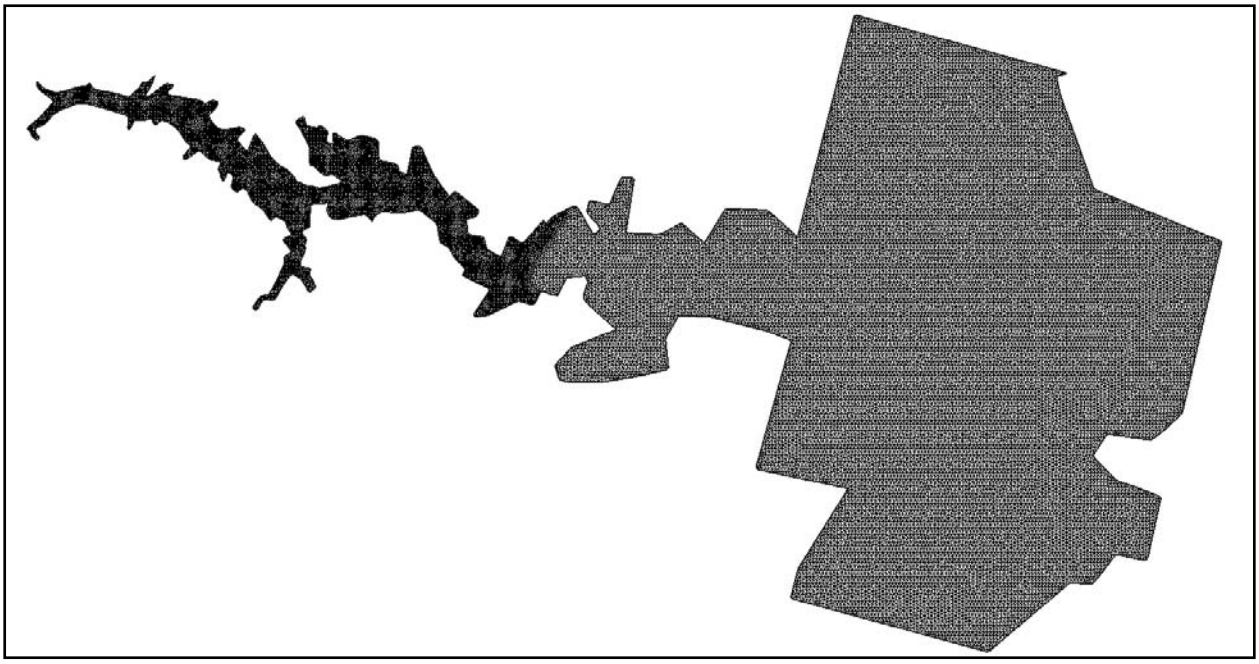

Figure 23. Malpasset dam mesh.

APPENDIX 2

Table 1: Dam Break Case 1 – Model time comparison for ADH and PTC-SER-ADH.

Model	ADH	PTC-SER-ADH
Number of Iterations	5	5
Initial Time Step (s)	0.09	0.09
Final Time Step (s)	0.5	0.5
Time to Completion (s)	418	300

Table 2: Dam Break Case 2 – Model time comparison for ADH and PTC-SER-ADH.

Model	ADH	PTC-SER-ADH
Number of Iterations	5	5
Initial Time Step (s)	0.009	0.009
Final Time Step (s)	0.25	0.25
Time to Completion (s)	1020	420

Table 3: Dam Break Case 3 – Model time comparison for ADH and PTC-SER-ADH.

Model	ADH	PTC-SER-ADH
Number of Iterations	5	5
Initial Time Step (s)	0.01	0.01
Final Time Step (s)	0.25	0.25
Time to Completion (s)	35	10

Table 4: Malpasset Dam Break Test Case – Water surface elevation comparisons.

Maximum Water Level (m)									
Gage	**P1**	**P2**	**P3**	**P4**	**P5**	**P6**	**P7**	**P8**	**P9**
Simulated	85.5	87.2	55.2	64.2	45.9	43.6	44.1	37.9	33.1
Observed	85.2	87.2	54.9	64.7	46.3	43.8	44.4	38.6	31.9
Gage	**P10**	**P11**	**P12**	**P13**	**P14**	**P15**	**P16**	**P17**	**S6**
Simulated	39.7	25.0	26.1	21.2	20.2	19.0	17.4	14.2	85.0
Observed	40.7	24.2	24.9	21.0	20.7	18.6	17.2	14.0	84.2
Gage	**S7**	**S8**	**S9**	**S10**	**S11**	**S12**	**S13**	**S14**	
Simulated	50.3	53.9	47.1	35.4	26.7	20.9	17.1	13.0	
Observed	49.1	54	46	34.9	27.4	21.5	16.1	12.9	

Table 5: Malpasset Dam Break Test Case: Travel time between transformers.

Travel time (seconds)		
Transformer	**A to B**	**B to C**
Simulated	1150	165
Observed	1140	180

Table 6: Malpasset Dam Break Test Case- Model time comparison for ADH and PTC-SER-ADH.

Model	**ADH**	**PTC-SER-ADH**
Number of Iterations	4	4
Initial Time Step (s)	0.1	0.1
Final Time Step (s)	50	50
Time to Completion (s)	1050	600